



The role of magnetization in phase-ordering kinetics of the short-range and long-range Ising model

Wolfhard Janke^{1,a}, Henrik Christiansen^{1,2,b}, and Suman Majumder^{1,3,c}

¹ Institut für Theoretische Physik, Universität Leipzig, IPF 231101, 04081 Leipzig, Germany

² Present Address: NEC Laboratories Europe GmbH, Kurfürsten-Anlage 36, 69115 Heidelberg, Germany

³ Amity Institute of Applied Sciences, Amity University Uttar Pradesh, Noida 201313, India

Received 1 February 2023 / Accepted 12 May 2023 / Published online 26 June 2023
© The Author(s) 2023

Abstract The kinetics of phase ordering has been investigated for numerous systems via the growth of the characteristic length scale $\ell(t) \sim t^\alpha$ quantifying the size of ordered domains as a function of time t , where α is the growth exponent. The behavior of the squared magnetization $\langle m(t)^2 \rangle$ has mostly been ignored, even though it is one of the most fundamental observables for spin systems. This is most likely due to its vanishing for quenches in the thermodynamic limit. For finite systems, on the other hand, we show that the squared magnetization does not vanish and may be used as an easier to extract alternative to the characteristic length. In particular, using analytical arguments and numerical simulations, we show that for quenches into the ordered phase, one finds $\langle m(t)^2 \rangle \sim m_0^2 t^{d\alpha}/V$, where m_0 is the equilibrium magnetization, d the spatial dimension, and V the volume of the system.

1 Introduction

Phase-ordering kinetics is omnipresent in nature and a very general phenomenon [1–3]. It occurs in many physical situations, e.g., when quenching a system from a disordered state at high temperature to a low temperature where in equilibrium it would be in an ordered state. In case of spin models such as the Ising model, this corresponds to a nonequilibrium relaxation from the paramagnetic to a ferromagnetic state. During this process, one observes the growth of ordered regions (or domains) with time t which is driven by the reduction of the total area of domain walls, as every domain wall contributes energetically. The goal is to quantify this phase-ordering process. Usually this is achieved by investigating the characteristic length scale $\ell(t)$ as a measure for the average linear extent of the domains, which typically grows like a power-law $\ell(t) \sim t^\alpha$. We show that instead of measuring $\ell(t)$, one may alternatively investigate the conceptually much easier squared magnetization $\langle m(t)^2 \rangle$ during this process; a quantity apparently overlooked in the past as being interesting.

Henrik Christiansen and Suman Majumder contributed equally to this work.

^a e-mail: wolfhard.janke@itp.uni-leipzig.de (corresponding author)

^b e-mail: henrik.christiansen@itp.uni-leipzig.de

^c e-mail: smajumder@amity.edu

We find $\langle m(t)^2 \rangle \sim \ell(t)^d \sim t^{d\alpha}$, both from our analytical arguments as well as from simulations of the Ising model with nearest-neighbor interactions and the long-range Ising model with power-law interactions in one and two dimensions. This should not be confused with the zero-field-cooled or thermoremanent magnetization in the response of the system after quenching with an applied (small) magnetic field [4–7]. While the equilibrium and nonequilibrium properties of the nearest-neighbor Ising model are, a priori, extremely well studied, both properties are not studied to the same extent in the long-range model. The Ising model with long-range interactions is of special interest, as it allows one to tune the interaction range, thereby serving as a generic model for long-range interactions that are omnipresent in natural and other sciences, ranging from electrostatic forces over neuroscience to economical phenomena [8–12].

2 Model and methods

The nearest-neighbor Ising model (NNIM) has the ubiquitous Hamiltonian

$$\mathcal{H} = -J_0 \sum_{\langle i, j \rangle} s_i s_j, \quad (1)$$

where $s_i = \pm 1$ are Ising spins, J_0 is the coupling strength, and $\langle i, j \rangle$ symbolizes summation over only the

nearest neighbors of a d -dimensional (hypercubic) lattice. We use periodic boundary conditions to minimize boundary effects so that spins at opposing boundaries interact with each other as if they were nearest neighbours. As an extension to this model, we consider the long-range Ising model (LRIM) with Hamiltonian

$$\mathcal{H} = -\frac{1}{2} \sum_i \sum_j J(|\vec{r}_i - \vec{r}_j|) s_i s_j, \quad (2)$$

with J chosen to decay according to a power law, that is

$$J(|\vec{r}_i - \vec{r}_j|) = \frac{J_0}{|\vec{r}_i - \vec{r}_j|^{d+\sigma}}, \quad (3)$$

where d is the spatial dimension and $\sigma > 0$ can be tuned to capture different long-range behavior. For $\sigma \leq 0$, the potential (without further normalization) diverges. This case will not be considered here. To mitigate the strong finite-size effects of this long-range model as much as possible, we will use Ewald summation to calculate effective interaction strengths J [13–15] over the minimum image convention often associated with periodic boundary conditions. Both models are investigated in $d = 1$ and $d = 2$ (on square $L \times L$ lattices). In our simulations J_0 sets the unit of energy and J_0/k_B the unit of temperature where k_B is the Boltzmann constant (i.e., we set $J_0 = k_B = 1$ for convenience).

The system is simulated using Monte Carlo (MC) simulations. One of the big advantages of MC simulations in equilibrium is that one may use collective updates in which many degrees of freedom are updated at once. Especially successful for spin models with both nearest-neighbor and long-range interactions are cluster algorithms [14, 16–20]. For nonequilibrium studies, it is, however, important to only perform physical and thereby local moves, so that one is restricted to single-spin flip dynamics. The computational complexity for a single spin flip scales as $\mathcal{O}(1)$ in the NNIM, but as $\mathcal{O}(N)$ in the LRIM since all $N \equiv V = L^d$ spins interact with each other. Exploiting the observation that during a sweep (which consists of N single-spin flip attempts) only a small fraction of spins is updated, we were able to significantly lower the prefactor of this scaling by a factor $\sim 10^3$ [15, 21]. This allows us to simulate rather big systems of size N up to 4096^2 , which was sufficient for the present purpose. For a recently developed much faster but more involved hierarchical and adaptive tree-like single-spin update algorithm that is compatible with $\mathcal{O}(\log N)$ complexity, see Refs. [22, 23].

The simulation protocol in our phase-ordering kinetics study is to prepare an initial disordered configuration with magnetization $m = \sum_i s_i / V \approx 0$. Subsequently, we quench the system below the critical temperature T_c , where the system is ferromagnetic. The process occurring is driven by the reduction of energetically unfavorable domain boundaries, where eventually at late times, one of the two magnetic branches with m fluctuating around $\pm m_0$ is “randomly” selected

with m_0 denoting the equilibrium magnetization at the quench temperature.

3 Results

We start our analysis by presenting in Fig. 1 snapshots during the phase-ordering process in $d = 2$ of the NNIM compared to the LRIM with $\sigma = 0.6$ for a quench from a randomly drawn disordered configuration at $T = \infty$ to $T = 0.1T_c$, where $T_c(\sigma)$ for the LRIM was extracted from Ref. [14]. Phenomenologically, the events appear similar and in both systems, the domains grow with time. While in the NNIM, the domains form with very smooth boundaries, for the LRIM, one observes more often relatively sharp corners, especially at late times. Apparent are of course the different time scales involved. For the NNIM, the lattice is close to be aligned at $t \approx 10^5$ (in units of sweeps), whereas in the LRIM, the same is observed already at $t \approx 10^3$. There could be different reasons for this: (i) a larger amplitude in the LRIM, (ii) a different growth exponent, or (iii) a combination of both.

3.1 Characteristic length

Therefore, in phase-ordering kinetics, one is mainly interested in the quantification of the growth of domains consisting of ordered regions with time. This can be quantified by measuring the characteristic length scale $\ell(t)$ of the average domain size. It is known that for the NNIM one has a power-law growth

$$\ell(t) \sim t^\alpha, \quad (4)$$

with $\alpha = 1/z = 1/2$, where $z = 2$ is the usual equilibrium dynamical exponent [24, 25]. For the nonequilibrium behavior of the LRIM, there exists a long-standing

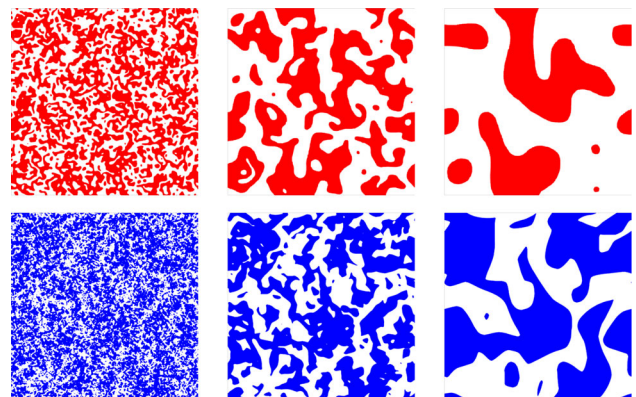


Fig. 1 Snapshots for the phase-ordering kinetics of the NNIM (upper panel, red) with quench temperature $T = 0.1T_c = 0.2269$ and $L = 4096$ at times $t = 10^3, 10^4, 10^5$ (in units of sweeps) and LRIM (lower panel, blue) with $\sigma = 0.6$, $T = 0.1T_c(\sigma) = 1.2555$ [14], and $L = 4096$ at $t = 20, 200, 1000$ from left to right

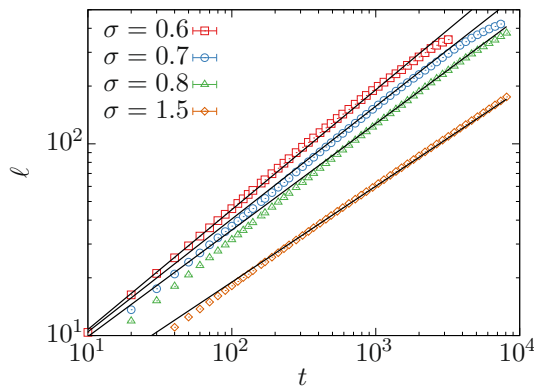


Fig. 2 Characteristic length scale $\ell(t)$ for the $d = 2$ LRIM on a log-log scale. Shown are the cases $\sigma = 0.6, 0.7, 0.8,$ and 1.5 for linear system size $L = 4096$. The black straight lines indicate the expected power-law growth as predicted by Eq. (5)

prediction for the growth of the characteristic length based on continuum descriptions of this model [26–28]:

$$\ell(t) \sim \begin{cases} t^{1/2} & \sigma > 1 \\ (t \ln t)^{1/2} & \sigma = 1, \\ t^{1/(1+\sigma)} & \sigma < 1 \end{cases} \quad (5)$$

where for $\sigma > 1$, one has the same growth exponent $\alpha = 1/2$ as in the NNIM. This scaling law does not depend on the spatial dimension d and has been numerically confirmed by us in $d = 2$ [15, 21] and subsequently also settled to be valid in $d = 1$ [29].

In our studies, we extracted the values of the characteristic length from the decay of the equal-time two-point correlation function

$$C(\vec{r}, t) = \langle s_i s_j \rangle - \langle s_i \rangle \langle s_j \rangle, \quad (6)$$

where $\langle \dots \rangle$ stands for an average over different initial (disordered) configurations and time evolutions and \vec{r} is the distance between the locations of the spins s_i and s_j . To get an appropriate estimate of $\ell(t)$, we take the intersection of $\bar{C}(r, t)$ ($= C(\vec{r}, t)$ averaged over all directions) with a constant value $c \in (0, 1)$ (we choose $c = 0.5$). This method is rather involved and has the drawback that for an efficient calculation of the correlation function, one has to make use of a fast Fourier transform [30, 31] to calculate $\langle s_i s_j \rangle$.

In Fig. 2, we show the characteristic length for the $d = 2$ LRIM with $\sigma = 0.6, 0.7, 0.8,$ and 1.5 . The system was prepared in a disordered configuration and quenched to $T = 0.1T_c(\sigma)$ as explained above. Here, we present new data for large systems of linear size up to $L = 4096$ and average over 50 independent time evolutions. For the values of σ that are in the long-range regime, a growth with $\alpha = 1/(1 + \sigma)$ is expected, whereas for $\sigma > 1$, one expects $\alpha = 1/2$. As can be seen from the log-log plots of this figure, the data are consistent with this prediction depicted by the black solid

lines. This is a reconfirmation of our results previously reported for up to $L = 2048$ [15, 21].

3.2 Magnetization

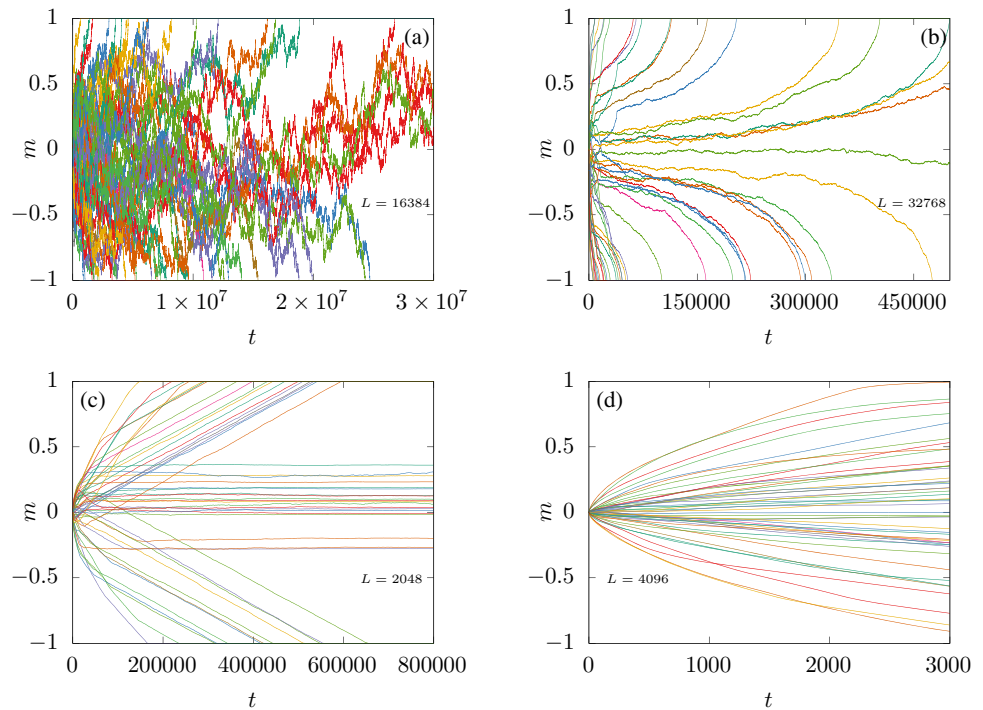
In the paramagnetic phase in equilibrium, one trivially has $\langle m(T) \rangle = 0$ since the entropic contributions dominate, where $m = \sum_i s_i / V$ is the usual magnetization. Below the critical temperature, in the ferromagnetic phase, the spontaneous magnetization $m_0(T) \neq 0$, i.e., one in practice observes $\langle |m(T)| \rangle \approx m_0$. However, due to the \mathcal{Z}_2 symmetry, for finite systems in equilibrium, one still in principle has $\langle m(T) \rangle = 0$. In practice, this is often not observed in equilibrium simulations for large systems since there is a first-order transition between the magnetic branches below T_c suppressing the crossover. During a quench from the paramagnetic phase to the ferromagnetic phase, m of finite systems goes for each individual run from the initial magnetization $m \approx 0$ in the disordered state¹ into one of the two ordered branches with $m = \pm m_0(T)$ ($\approx \pm 1$ for low T), where the sign is realized randomly for each run. This means that for the time evolution of the expectation value of the magnetization, one has $\langle m(t) \rangle = 0$. What is nonzero, however, is the expectation value of the squared magnetization $\langle m(t)^2 \rangle$ as a function of time since each individual run still evolves into one of the magnetization branches.

In Fig. 3, we present these individual time evolutions of the magnetization following a quench in the ordered region. In total, we have run 500 independent time evolutions for the $d = 1$ NNIM, 150 for the $d = 1$ LRIM, and 50 for the $d = 2$ NNIM and LRIM, respectively. The $d = 1$ model is shown in (a) for the NNIM and in (b) for the LRIM with $\sigma = 0.6$. Plots (c) and (d) are the analog plots for $d = 2$. The quench temperature was generally chosen to be $T = 0.1T_c$ with the “exception” of the $d = 1$ NNIM in (a) where this choice degenerates to $T = 0$.² It is apparent that in most cases, roughly 50% of the runs choose a positive magnetization, whereas the other 50% are negatively magnetized. The trajectories for all four different systems look very different. While the time evolutions of the magnetization for the $d = 1$ NNIM more or less resemble a “random walk”, the curves for the corresponding LRIM look much more directed. In some of the simulations, configurations occur that get “stuck” into a (strictly speaking meta-stable) striped state configuration as can be appreciated from the curves that are roughly constant at $m \neq \pm 1$. This is a well-known phenomenon for the $d = 2$ NNIM (especially at zero temperature) [34] and has recently also been investigated in the LRIM [35].

¹In simulations, there exists a choice of starting the simulation using $m \equiv 0$ (“microcanonical”) or $m \approx 0$ (“canonical”). Here we have used $m \approx 0$.

²The $d = 1$ NNIM is only ordered at $T = 0$, so that formally $T_c = 0$. The critical temperature $T_c = 2 / \ln(1 + \sqrt{2})$ for the $d = 2$ NNIM is well known [32]. For the LRIM, there exist numerical studies in $d = 1$ [33] and $d = 2$ [14] from where we have extracted T_c .

Fig. 3 Magnetization m versus time t in $d = 1$ for **a** the NNIM and **b** the LRIM with $\sigma = 0.6$, whereas **c** and **d** show the analogous data in $d = 2$. For the $d = 1$ NNIM we used $T = 0$ and for all other cases $T = 0.1T_c$ as our quench temperature. For details, see text. Note the (very) different time scales of the plots



We now present an analytic argument for the growth of the expectation value of the squared magnetization $\langle m(t)^2 \rangle$, which is clearly nonzero from above data. Since we know that the average linear domain size scales with time t as $\ell(t) \sim t^\alpha$, the average volume of a domain scales in d dimensions as

$$V_d(t) \sim \ell(t)^d \sim t^{d\alpha}, \tag{7}$$

so that the average number of domains in a total volume $V = L^d$ is given by

$$N_d(t) \sim V/V_d(t) \sim (L/\ell(t))^d. \tag{8}$$

Next, assume that a configuration at time t consists of $N_d(t)$ domains of linear sizes ℓ_d whose mean is $\ell(t)$ such that $N_d(t)\ell(t)^d \sim V$. This can be achieved by writing the probability distribution $P(\ell_d, t)$ of linear domain sizes ℓ_d in the dynamical scaling form

$$P(\ell_d, t) = \ell(t)^{-1} f(\ell_d/\ell(t)) \tag{9}$$

where the scaling function $f(x)$ satisfies $\int_0^\infty dx f(x) = 1$ and $\langle x \rangle \equiv \int_0^\infty dx x f(x) = 1$. The first condition implies that $P(\ell_d, t)$ is normalized to unity and the second condition leads to the desired property that

$$\langle \ell_d(t) \rangle \equiv \int_0^\infty d\ell_d \ell_d P(\ell_d, t) = \langle x \rangle \ell(t) = \ell(t). \tag{10}$$

Higher-order moments scale similarly with $\ell(t)$ as

$$\langle \ell_d(t)^n \rangle \equiv \int_0^\infty d\ell_d \ell_d^n P(\ell_d, t) = \langle x^n \rangle \ell(t)^n. \tag{11}$$

The total magnetization $M(t) = Vm(t)$ results by summing up the $N_d(t)$ contributions

$$M_d = \pm V_d m_0, \tag{12}$$

where the sign ± 1 is random and it is assumed that each domain has already equilibrated locally to the spontaneous magnetization density $m_0(T)$ at $T < T_c$. Due to the random sign, $M(t) = \sum_{i=1}^{N_d} M_d$ of each time evolution is equally likely positive or negative so that $\langle M(t) \rangle = 0$. For the squared magnetization, all contributions add up and by a random-walk argument (with $M(t)$ playing the role of the end-to-end distance), one obtains $\langle M(t)^2 \rangle = N_d \langle M_d^2 \rangle$. Using $V_d \sim \ell_d^d$ and (11) gives

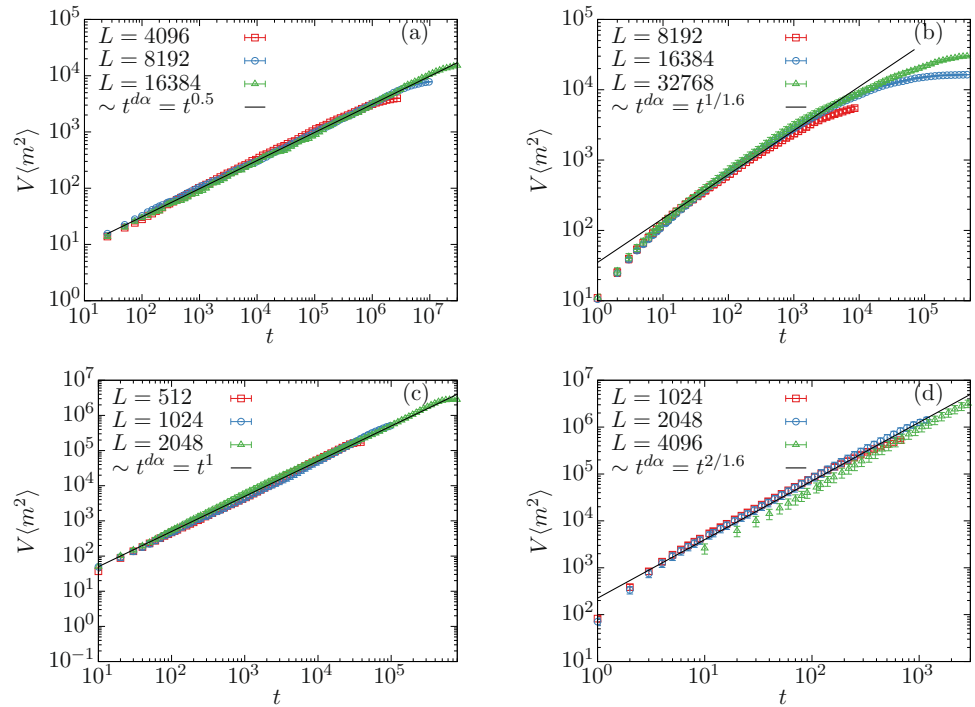
$$\langle M(t)^2 \rangle \sim N_d m_0^2 \langle x^{2d} \rangle \ell(t)^{2d} \sim V m_0^2 \ell(t)^d \tag{13}$$

which implies for $m(t) = M(t)/V$

$$\langle m(t)^2 \rangle \sim m_0^2 \frac{\ell(t)^d}{V} \sim m_0^2 \frac{t^{d\alpha}}{V}. \tag{14}$$

This result confirms that the squared magnetization is zero in the limit $V \rightarrow \infty$, as one would expect for a global quantity. It is the amplitude of the leading finite-size scaling correction that carries the signature of the growing length scale. Note that a similar power-law

Fig. 4 Shown is $V\langle m(t)^2 \rangle$ versus t after a quench into the ordered phase in $d = 1$ for **a** the NNIM and **b** the LRIM with $\sigma = 0.6$. The other panels **c** and **d** show analogous data for $d = 2$



scaling behavior is known from the critical short-time dynamics following a quench from a disordered initial state with vanishing magnetization to the *critical* point of a system: $\langle m(t)^2 \rangle \sim t^{(d-2\beta/\nu)}/z/V$ where β and ν are the critical exponents of the magnetization and correlation length, respectively, and z is the dynamical critical exponent [36, 37]. Putting formally $\beta/\nu = 0$ for a non-critical quench to temperatures below the critical temperature and identifying $1/z = \alpha$ with its non-critical value, Eq. (14) is recovered. Even though the physical situations are quite different, the origin of the similar scaling behavior can be traced to the applicability of the random-walk argument (or central limit theorem) in both cases.

The simplest but unrealistic realization of the dynamic scaling function in (9) would be $f(x) = \delta(x-1)$ (with $\langle x^n \rangle = 1$) which corresponds to assuming that all N_d domain sizes are equal, $\ell_d = \ell(t)$, so that the random-walk picture assumes its simplest form. A pure exponential, $f(x) = e^{-x}$ (with $\langle x^n \rangle = n!$), is clearly a more realistic ansatz. Empirically an even better choice [38] is the double exponential $f(x) = a(e^{-\frac{2ax}{a+1}} - e^{-\frac{2ax}{a-1}})$, parameterized by the constant a . For $a = 2$, it fits numerical data for the two-dimensional nearest-neighbor Blume–Capel model very well [38]. For this parameter choice, $f(x)$ steeply increases for small x as $16x/3$, develops a peak at $x_{\max} = (3/8)\ln 3$ of height $f_{\max} = 4/(3\sqrt{3})$, and for large x decays exponentially as $2e^{-4x/3}$. Recall that the Blume–Capel model is a spin-1 model with $s_i = \pm 1$ and 0, where the vacancies $s_i = 0$ can be suppressed by a large crystal-field coupling so that in this limit the model becomes equivalent to the Ising model.

A simpler, less microscopic argument goes as follows. The dynamical scaling properties of the coarsening process imply in general that $C(\vec{r}, t)$ depends only on the scaling variable $\vec{r}/\ell(t)$ but not on \vec{r} and t separately. This in turn implies that the structure factor, its Fourier transform $S(\vec{k}, t) = \int d\vec{r} C(\vec{r}, t) e^{i\vec{k}\vec{r}}$, exhibits the dynamic scaling behavior $S(\vec{k}, t)/\ell(t)^d = f(\vec{k}\ell(t))$. Since this does not depend on t as $k \rightarrow 0$ and a direct calculation yields the usual result $S(\vec{k} = \vec{0}, t) = V\langle m(t)^2 \rangle$ (recall that $\langle m \rangle = \langle s_i \rangle = 0$), one concludes that $\langle m(t)^2 \rangle \sim \ell(t)^d/V$, in agreement with the prediction (14) based on microscopic arguments.

We now check the prediction in Eq. (14) numerically: The upper two subplots of Fig. 4 show $V\langle m(t)^2 \rangle$ versus t in $d = 1$ after a quench to (a) $T = 0$ for the NNIM and (b) $T = 0.1T_c$ for the LRIM with $\sigma = 0.6$. The other subplots (c) and (d) show the analogous data for $d = 2$. Here, instead of $\langle m(t)^2 \rangle$, we have plotted $V\langle m(t)^2 \rangle$ to check for the predicted prefactor in (14). The factor m_0^2 is non-universal and dependent on temperature. We find in all cases that the data for different system sizes collapse reasonably well onto each other, confirming the prefactor of the prediction. In particular they agree well with the predicted time dependence drawn as a solid line with the theoretical slope (and adjusted amplitude). Furthermore, adapting the recipe of Ref. [39], we have verified that least-square fits using the ansatz $V\langle m(t)^2 \rangle = at^{d\alpha}$ provide estimates for the growth exponent α that are compatible with the theoretical expectations within a few percent accuracy. Details of this quite elaborate fitting exercise are discussed in the Appendix.

The big advantage of analyzing $\langle m(t)^2 \rangle$ is of course that this is extremely easy to calculate compared to

the rather involved estimation of $\ell(t)$ via the correlation function. When compared to the estimation of $\ell(t)$ via counting the spin sign-changes it is not (overly) sensitive to single thermally excited spins, either. One of the drawbacks is, however, that this quantity has significantly larger error bars.

4 Conclusion

We have investigated the behavior of the (squared) magnetization following a quench from a disordered state into the ordered phase, which is an often overlooked quantity during coarsening. While for finite systems of size $V = L^d$, the average magnetization is zero, the average squared magnetization carries the signature of growing domains. Using analytical arguments, it is shown that $\langle m(t)^2 \rangle \sim \ell(t)^d/V$, i.e., the squared magnetization may be used as an alternative observable to quantify the coarsening of domains. The predicted time dependence is verified numerically in $d = 1$ and $d = 2$ both for the NNIM and the LRIM with $\sigma = 0.6$. We also confirm the prefactor $1/V$ of the growth, validating our prediction. Additionally, we have also presented new data for the growth of the characteristic length $\ell(t)$ itself for the $d = 2$ LRIM with $\sigma = 0.6, 0.7, 0.8$, and 1.5 for system sizes up to $L = 4096$ using for $\ell(t)$ the standard definition from the intercept of the equal-time two-point correlation function (with $c = 0.5$). It would be interesting to investigate the time dependence of the squared magnetization in other coarsening systems such as the XY model both in the short-range and long-range variant.

Acknowledgements This paper is dedicated to Professor Malte Henkel on the occasion of his 60th birthday, with whom we studied “aging in practice” over many years. Discussions with Malte have always been a great pleasure and inspiration for our work. We thank Fabio Müller for useful discussion. This project was funded by the Deutsche Forschungsgemeinschaft (DFG, German Research Foundation) under Grant no. 189 853 844 – SFB/TRR 102 (Project B04) and further supported by the Deutsch-Französische Hochschule (DFH-UFA) through the Doctoral College “L⁴” under Grant no. CDFa-02-07 and the Leipzig Graduate School of Natural Sciences “BuildMoNa”. S.M. thanks the Science and Engineering Research Board (SERB), Govt. of India for a Ramanujan Fellowship (File no. R.JF/2021/000044).

Author contribution statement

All authors whose names appear on the submission (1) made substantial contributions to the conception or design of the work; or the acquisition, analysis, or interpretation of data; or the creation of new software used in the work; (2) drafted the work or revised it critically for important intellectual content; (3) approved the version to be published; and (4) agree to be accountable for all aspects of the work in ensuring that questions

related to the accuracy or integrity of any part of the work are appropriately investigated and resolved.

Funding Open Access funding enabled and organized by Projekt DEAL. This work was funded by the Deutsche Forschungsgemeinschaft (DFG, German Research Foundation) under Grant no. 189 853 844—SFB/TRR 102 (Project B04) and further supported by the Deutsch-Französische Hochschule (DFH-UFA) through the Doctoral College “L⁴” under Grant no. CDFa-02-07 and the Leipzig Graduate School of Natural Sciences “BuildMoNa”. S.M. received funding from the Science and Engineering Research Board (SERB), Govt. of India through a Ramanujan Fellowship (File no. R.JF/2021/000044).

Availability of data and material The datasets generated during and/or analyzed during the current study are available from the corresponding author on reasonable request.

Code availability Not applicable.

Declarations

Conflict of interest None.

Ethics approval Not applicable.

Consent to participate Not applicable.

Consent for publication Not applicable.

Open Access This article is licensed under a Creative Commons Attribution 4.0 International License, which permits use, sharing, adaptation, distribution and reproduction in any medium or format, as long as you give appropriate credit to the original author(s) and the source, provide a link to the Creative Commons licence, and indicate if changes were made. The images or other third party material in this article are included in the article’s Creative Commons licence, unless indicated otherwise in a credit line to the material. If material is not included in the article’s Creative Commons licence and your intended use is not permitted by statutory regulation or exceeds the permitted use, you will need to obtain permission directly from the copyright holder. To view a copy of this licence, visit <http://creativecommons.org/licenses/by/4.0/>.

Appendix: Growth exponent α from least-square fitting

While the layout of our study primarily targeted on a qualitative confirmation of the predicted scaling behavior, we eventually also attempted to perform least-square fits to the data assuming the expected asymptotic functional dependence $V\langle m(t)^2 \rangle = at^{d\alpha}$ and $\ell(t) = at^\alpha$, which amounts to linear two-parameter fits.

We compared the results of fits with equal spacings in t and $\ln t$. Because logarithmic spacings give automatically a uniform weight to the data over the full fit

Table 1 Summary of fitted growth exponents α using the ansatz $V(m(t)^2) = at^{d\alpha}$ respectively $\ell(t) = at^\alpha$ (last line)

Model	L	$t_{\min, \max}$	dof	α	$\ln(a)$	χ_r^2	α_{\min}	α_{\max}	α_{av}
1D NNIM	16,384	$10^2, 10^6$	36	0.506(5)[9]	1.01(5)	0.33	0.497	0.507	0.505
1D LRIM	32,768	60, 3000	14	0.62(3)[6]	3.7(2)	0.12	0.579	0.683	0.627
2D NNIM	2048	$10^3, 10^6/2$	24	0.49(1)[1]	1.89(12)	0.24	0.475	0.495	0.487
2D LRIM	2048	$10, 10^3$	17	0.63(2)[2]	5.46(16)	0.056	0.612	0.649	0.628
2D LRIM	4096	$10, 10^3$	17	0.64(2)[1]	4.94(20)	0.002	0.637	0.646	0.642
2D LRIM	4096	$10, 10^3$	13	0.644(1)[8]	0.862(4)	0.18	0.636	0.650	0.645

The numbers in square brackets [...] indicate the systematic error due to the choice of the fit interval (read off from the last 3 columns). χ_r^2 stands short for χ^2/dof

interval, we finally opted for this latter choice using 10 t values per decade (we have explicitly checked that using 20 or more t values per decade does not significantly alter the parameter estimates). All fit results reported below refer to this case if not otherwise indicated. Another advantage of the logarithmic spacing is that the used t values are naturally widely spaced (in particular for larger t), so that correlations of the data for closeby times do not play such a prominent role (of course, for a high-precision study, one could deal with such correlations by jackknife blocking techniques which are, however, rather laborious and hence left for future work).

For both considered quantities, one expects corrections to asymptotic scaling for small times t and finite-size corrections for large times. Since these corrections are not taken into account in the fit ansatz, we have estimated their influence on the parameter estimates by systematically varying both ends of the fit interval $t \in [t_{\min}, t_{\max}]$ over a rather wide range.

In the following, we go through the data presented in Fig. 4a–d point by point:

(a) 1D NNIM:

For the largest considered lattice size $L = 16384$, we obtain from a fit over $t \in [10^2, 10^6]$ with 36 degrees of freedom (dof) covering 4 decades in t the estimates $\alpha = 0.506(5)$, $\ln(a) = 1.01(5)$, $a = 2.76(12)$ with chi-squared value per dof, $\chi^2/\text{dof} = 0.33$. Using for comparison equally spaced t values with $\Delta t = 2500$ in the same fit interval (with 397 dof) yields the compatible estimates of $\alpha = 0.508(4)$, $\ln(a) = 0.98(5)$, $a = 2.67(12)$ with $\chi^2/\text{dof} = 0.035$ (note that since for equally spaced t the spacing is much finer, the χ^2/dof value is stronger affected by the data correlations).

By varying the boundaries t_{\min} and t_{\max} of the fit interval over the range $t_{\min} = 100, 200, \dots, 1000$ and $t_{\max} = 100000, 200000, \dots, 1000000$, the estimates of α from the 100 fits vary between $\alpha_{\min} = 0.497$ and $\alpha_{\max} = 0.507$, with an average of $\alpha_{\text{av}} = 0.505$. Thus, quoting $\alpha = 0.506(5)[9]$ (where the number “[9]” in square brackets roughly indicates the systematic uncertainty) is a rather conservative estimate agreeing with

the theoretically expected value of $\alpha = 1/2$ within 2–3% accuracy. All estimates of α are collected in Table 1.

(b) 1D LRIM ($\sigma=0.6$):

A glance on the data for the 1D LRIM in Fig. 4b shows that here the situation is more difficult. In particular, the finite-size corrections creep in much more gradually than for the 1D NNIM and even for the large lattice size $L = 32768$ they obviously start to become important already for $t \approx 5 \times 10^3$. This limits the available asymptotic fitting range substantially. A quite conservative fit interval is $t \in [60, 3000]$, still covering more than 1.5 decades in t . This gives $\alpha = 0.62(3)$, $\ln(a) = 3.7(2)$, $a = 41(7)$ with an acceptable $\chi^2/\text{dof} = 0.12$ for 14 dof.

Varying the fit boundaries $t_{\min} = 20, 30, \dots, 100$ and $t_{\max} = 1000, 2000, \dots, 5000$, we obtain from the 90 fits $\alpha_{\min} = 0.579$, $\alpha_{\max} = 0.683$, and $\alpha_{\text{av}} = 0.627$. The large spread in α reflects that for the 1D LRIM the asymptotic regime can hardly be identified. As final result we quote $\alpha = 0.62(3)[6]$. The agreement with the theoretical prediction $\alpha = 1/1.6 = 0.625$ is (apparently) excellent, but this should be taken with great care since the overall uncertainty of about 15% is relatively high in this case.

(c) 2D NNIM:

For the $L = 2048$ data, a fit over $t \in [1000, 500000]$ covering 2.5 decades in t yields the estimates $\alpha = 0.49(1)$, $\ln(a) = 1.89(12)$, $a = 6.62(85)$ with $\chi^2/\text{dof} = 0.24$ for 24 dof.

Varying the fit boundaries $t_{\min} = 100, 200, \dots, 1000$ and $t_{\max} = 100000, 150000, \dots, 500000$, we get from the 90 fits $\alpha_{\min} = 0.475$, $\alpha_{\max} = 0.495$, and $\alpha_{\text{av}} = 0.487$. Our final estimate $\alpha = 0.49(1)[1]$ hence verifies the theoretical prediction $\alpha = 1/2$ with an overall accuracy of 4%.

(d) 2D LRIM ($\sigma=0.6$):

For the 2D LRIM, the data for the largest lattice size $L = 4096$ shown in Fig. 4d looks somewhat off the trend for the smaller lattices. We have checked that this behavior is reproduced when averaging over different start configurations and time evolutions (and also when employing a completely independent computer code).

We therefore analyzed here $L = 2048$ and $L = 4096$ separately, and in the latter case extracted α also from the scaling of the characteristic length $\ell(t)$ for comparison.

For $L = 2048$, a fit over $t \in [10, 1000]$ covering 2 decades in t gives the estimate $\alpha = 0.63(2)$, $\ln(a) = 5.46(16)$, $a = 235(40)$ with a rather small $\chi^2/\text{dof} = 0.056$ for 17 dof.

Varying the fit boundaries $t_{\min} = 5, 10, \dots, 50$ and $t_{\max} = 500, 600, \dots, 1000$, we obtain from 60 fits $\alpha_{\min} = 0.612$, $\alpha_{\max} = 0.649$, and $\alpha_{\text{av}} = 0.628$. The final estimate $\alpha = 0.63(2)[2]$ agrees well with the prediction $\alpha = 1/1.6 = 0.625$ with an accuracy of about 6%.

For $L = 4096$, a fit over the same range $t \in [10, 1000]$ yields $\alpha = 0.64(2)$, $\ln(a) = 4.94(20)$, $a = 140(30)$ with an even smaller $\chi^2/\text{dof} = 0.002$ for 17 dof.

Varying here the fit boundaries over a larger range, $t_{\min} = 5, 10, \dots, 100$ and $t_{\max} = 500, 600, \dots, 2000$, the 320 fits yield $\alpha_{\min} = 0.637$, $\alpha_{\max} = 0.646$, and $\alpha_{\text{av}} = 0.642$. As final estimate, we quote $\alpha = 0.64(2)[1]$ with an accuracy of about 4–5%.

Thus, also for the $L = 4096$ data, the scaling exponent α turns out to be consistent with the theoretical prediction $\alpha = 0.625$, which supports the visual impression of Fig. 4d that the $L = 4096$ data are mainly shifted vertically compared to the smaller lattices.

Characteristic length $\ell(t)$: For the 2D LRIM with $\sigma = 0.6$, we have also performed fits to the hitherto unpublished data of $\ell(t)$ for $L = 4096$ shown in Fig. 2. For comparison with the magnetization data, we chose the same fit interval $t \in [10, 1000]$. This fit gives $\alpha = 0.644(1)$, $\ln(a) = 0.862(4)$, $a = 2.37(1)$ with $\chi^2/\text{dof} = 0.18$ for 13 dof. The estimate for α is compatible with that from the magnetization data, but in units of the here much smaller statistical error, it is quite a bit larger than the theoretically expected value of $\alpha = 1/1.6 = 0.625$.

Varying here the fit boundaries $t_{\min} = 10, 20, \dots, 100$ and $t_{\max} = 500, 600, \dots, 1000$, we get from the 60 fits $\alpha_{\min} = 0.636$, $\alpha_{\max} = 0.650$, and $\alpha_{\text{av}} = 0.645$. As conservative final estimate, one may take $\alpha = 0.644(1)[8]$, which appears rather accurate (0.16% statistical and 1.25% systematic error, 1.5% total uncertainty)—but within error bars it is clearly off the theoretical expectation (the deviation from the theoretical prediction $\alpha = 1/1.6 = 0.625$ is 3.0%). However, compared to $\alpha = 0.63(2)[2]$ and $\alpha = 0.64(2)[1]$ from the magnetization data for $L = 2048$ and $L = 4096$, the estimate of α extracted from $\ell(t)$ is fully compatible. Mainly due to the much smaller statistical error by a factor of about 10–20, it appears much less compatible with the theoretical value.

Our raw data clearly show that the relative errors of the magnetization decrease with t , whereas for $\ell(t)$ obtained via the correlation function they do increase with t . We have determined $\ell(t)$ only for the 2D LRIM, but the observed trend should be general. In error

weighted fits, this gives for the magnetization implicitly a higher weight to the asymptotic region of large times t .

On an absolute scale, the statistical errors for $\ell(t)$ are, however, considerably smaller (which is consistent with the apparent better accuracy of the α estimate from $\ell(t)$): For the 2D LRIM with $L = 4096$ a factor of ≈ 10 at time $t = 1000$ and ≈ 100 for small times $t \lesssim 100$ –200.

We hence conclude that estimating the growth exponent α from the characteristic length scale $\ell(t)$ is (to our own surprise) not more reliable than using the magnetization, which is much easier to measure. Even though the raw data for $\ell(t)$ are much more precise, the systematic uncertainties due to neglected corrections for small and large t are of the same order as for the magnetization and apparently harder to control. Overall this does not permit a more reliable estimate of α from $\ell(t)$.

References

1. A.J. Bray, Theory of phase-ordering kinetics. *Adv. Phys.* **51**, 481 (2002)
2. S. Puri, V. Wadhawan (eds.), *Kinetics of Phase Transitions* (CRC Press, Boca Raton, 2009)
3. M. Henkel, M. Pleimling, *Non-Equilibrium Phase Transitions, Vol. 2: Ageing and Dynamical Scaling Far from Equilibrium* (Springer, Heidelberg, 2010)
4. M. Henkel, M. Pleimling, C. Godreche, J.-M. Luck, Aging, phase ordering, and conformal invariance. *Phys. Rev. Lett.* **87**, 265701 (2001)
5. F. Corberi, E. Lippiello, M. Zannetti, Scaling of the linear response function from zero-field-cooled and thermoremanent magnetization in phase-ordering kinetics. *Phys. Rev. E* **68**, 046131 (2003)
6. E. Lorenz, W. Janke, Numerical tests of local scale invariance in ageing q -state Potts models. *Europhys. Lett.* **77**, 10003 (2007)
7. M. Henkel, M. Pleimling, R. Sanctuary (eds.), *Ageing and the Glass Transition*, Lecture Notes in Physics, vol. 716 (Springer, Heidelberg, 2007)
8. P. Bak, *How Nature Works* (Oxford University Press, Oxford, 1997)
9. T. Lux, M. Marchesi, Scaling and criticality in a stochastic multi-agent model of a financial market. *Nature* **397**, 498 (1999)
10. J.M. Beggs, D. Plenz, Neuronal avalanches in neocortical circuits. *J. Neurosci.* **24**, 11167 (2003)
11. O. Petrs, D. Neelin, Critical phenomena in atmospheric precipitation. *Nat. Phys.* **2**, 393 (2006)
12. J. Gundh, A. Singh, R.K.B. Singh, Ordering dynamics in neuron activity pattern model: an insight to brain functionality. *PLoS One* **10**, 0141463 (2015)
13. P. Ewald, Die Berechnung optischer und elektrostatischer Gitterpotentiale. *Ann. Phys. (Berl.)* **369**, 253 (1921)
14. T. Horita, H. Suwa, S. Todo, Upper and lower critical decay exponents of Ising ferromagnets with long-range interaction. *Phys. Rev. E* **95**, 012143 (2017)

15. H. Christiansen, S. Majumder, W. Janke, Phase ordering kinetics of the long-range Ising model. *Phys. Rev. E* **99**, 011301 (2019)
16. R.H. Swendsen, J.-S. Wang, Nonuniversal critical dynamics in Monte Carlo simulations. *Phys. Rev. Lett.* **58**, 86 (1987)
17. U. Wolff, Collective Monte Carlo updating for spin systems. *Phys. Rev. Lett.* **62**, 361 (1989)
18. E. Luijten, H.W.J. Blöte, Monte Carlo method for spin models with long-range interactions. *Int. J. Mod. Phys. C* **06**, 359 (1995)
19. K. Fukui, S. Todo, Order- N cluster Monte Carlo method for spin systems with long-range interactions. *J. Comput. Phys.* **228**, 2629 (2009)
20. E. Flores-Sola, M. Weigel, R. Kenna, B. Berche, Cluster Monte Carlo and dynamical scaling for long-range interactions. *Eur. Phys. J. Spec. Top.* **226**, 581 (2017)
21. W. Janke, H. Christiansen, S. Majumder, Coarsening in the long-range Ising model: Metropolis versus Glauber criterion. *J. Phys. Conf. Ser.* **1163**, 012002 (2019)
22. F. Müller, H. Christiansen, S. Schnabel, W. Janke, Fast, hierarchical, and adaptive algorithm for Metropolis Monte Carlo simulations of long-range interacting systems. *Phys. Rev. X* (to appear) (2023). [arXiv:2207.14670](https://arxiv.org/abs/2207.14670)
23. F. Müller, H. Christiansen, W. Janke, Phase-separation kinetics in the two-dimensional long-range Ising model. *Phys. Rev. Lett.* **129**, 240601 (2022)
24. I.M. Lifshitz, Kinetics of ordering during second-order phase transitions. *Sov. Phys. JETP* **15**, 939 (1962)
25. S.M. Allen, J.W. Cahn, A microscopic theory for antiphase boundary motion and its application to antiphase domain coarsening. *Acta Metall.* **27**, 1085 (1979)
26. A.J. Bray, Domain-growth scaling in systems with long-range interactions. *Phys. Rev. E* **47**, 3191 (1993)
27. A.J. Bray, A.D. Rutenberg, Growth laws for phase ordering. *Phys. Rev. E* **49**, R27 (1994)
28. A.D. Rutenberg, A.J. Bray, Phase-ordering kinetics of one-dimensional nonconserved scalar systems. *Phys. Rev. E* **50**, 1900 (1994)
29. F. Corberi, E. Lippiello, P. Politi, One dimensional phase-ordering in the Ising model with space decaying interactions. *J. Stat. Phys.* **176**, 510 (2019)
30. J.W. Cooley, J.W. Tukey, An algorithm for the machine calculation of complex Fourier series. *Math. Comput.* **19**, 297 (1965)
31. M.E.J. Newman, G.T. Barkema, *Monte Carlo Methods in Statistical Physics* (Oxford University Press, Oxford, 1999)
32. L. Onsager, Crystal statistics. I. A two-dimensional model with an order-disorder transition. *Phys. Rev.* **65**, 117 (1944)
33. Z. Glumac, K. Uzelac, Finite-range scaling study of the 1d long-range Ising model. *J. Phys. A: Math. Gen.* **22**, 4439 (1989)
34. V. Spirin, P. Krapivsky, S. Redner, Fate of zero-temperature Ising ferromagnets. *Phys. Rev. E* **63**, 036118 (2001)
35. R. Agrawal, F. Corberi, F. Insalata, S. Puri, Asymptotic states of Ising ferromagnets with long-range interactions. *Phys. Rev. E* **105**, 034131 (2022)
36. T. Tomé, M.J. de Oliveira, Short-time dynamics of critical nonequilibrium spin models. *Phys. Rev. E* **58**, 4242 (1998)
37. E.V. Albano, M.A. Bab, G. Baglietto, R.A. Borzi, T.S. Grigera, E.S. Loscar, D.E. Rodriguez, M.I. Rubio Puzzo, G.P. Saracco, Study of phase transitions from short-time non-equilibrium behaviour. *Rep. Prog. Phys.* **74**, 026501 (2011)
38. K. Tafa, S. Puri, D. Kumar, Kinetics of domain growth in systems with local barriers. *Phys. Rev. E* **63**, 046115 (2001)
39. H. Christiansen, S. Majumder, M. Henkel, W. Janke, Aging in the long-range Ising model. *Phys. Rev. Lett.* **125**, 180601 (2020)